

Critical size for the generation of misfit dislocations and their effects on electronic properties in GaAs nanosheets on Si substrate

Zaoshi Yuan,^{1,2} Kohei Shimamura,^{1,3,4} Fuyuki Shimojo,^{1,3} and Aiichiro Nakano¹

¹*Collaboratory for Advanced Computing and Simulations, Department of Physics and Astronomy, Department of Computer Science, and Department of Chemical Engineering and Materials Science, University of Southern California, Los Angeles, California 90089-0242, USA*

²*Department of Chemical Engineering, Stanford University, Stanford, California 94305-5025, USA*

³*Department of Physics, Kumamoto University, Kumamoto 860-8555, Japan*

⁴*Department of Applied Quantum Physics and Nuclear Engineering, Kyushu University, Fukuoka 819-0395, Japan*

(Received 2 June 2013; accepted 5 August 2013; published online 21 August 2013)

While nanowires and nanosheets (NSs) grown on lattice-mismatched substrates have a number of promising technological applications such as solar cells, generation of misfit dislocations (MFDs) at their interfaces is a major concern for the efficiency of these devices. Here, combined molecular-dynamics and quantum-mechanical simulations are used to study MFDs at the interface between a GaAs NS and a Si substrate. Simulation results show the existence of a critical NS thickness, below which NSs are grown free of MFDs. The calculated critical thickness value is consistent with available experimental observations. Charge transfer at the MFD core is found to modify the electronic band profile at the GaAs/Si interface significantly. These effects should have profound impacts on the efficiency of lattice-mismatched NS devices. © 2013 AIP Publishing LLC. [<http://dx.doi.org/10.1063/1.4818957>]

I. INTRODUCTION

Semiconductor nanowires (NWs) have broad applications such as solar cells^{1,2} due to their unique physical properties at the nanometer scale.^{3–5} Most importantly, the NW configuration allows the growth of lattice-mismatched heterostructures due to its extensive strain-relief capability arising from efficient lateral stress relaxation. In particular, heterostructures composed of various semiconductors with different band gaps can be grown, which are otherwise impossible due to their different lattice constants. This significantly enlarges the design space for high-efficiency tandem solar cells, in which different materials absorb different parts of the solar spectrum to exceed the Shockley-Queisser limit⁶ for the solar-cell efficiency. Recently, NWs of various semiconductors such as GaAs/AlGaAs,^{7,8} InAs,⁹ GaAs/InAs,¹⁰ and InP (Ref. 11) have been grown on low-cost Si substrates using the vapor-liquid-solid method¹² and the selective-area metal organic vapor phase epitaxy.¹³ This has enhanced the viability of lattice-mismatched NW-based devices not only for solar cells but also for light-emitting diodes⁷ and vertical transistors.¹⁰

A major problem often encountered in semiconductor NWs is a large number of stacking defects such as twin boundaries, which may alter electronic properties and degrade device performance.^{14,15} Previous theoretical works suggested that stacking defects nucleate at the edge of the NW top surface.¹⁶ In the case of a GaAs NW grown in the [111]B direction, in particular, stacking defects nucleate preferentially at the corners of the hexagonal top surface.¹⁷ A twin-generation mechanism involving a triangular crystalline island on the NW top was also proposed for the [111]B GaAs NW.¹⁸ To alleviate the stacking-defect problem of

GaAs NWs, which presumably arise from the hexagonal NW geometry, a new architecture—nanosheet (NS)—has recently been proposed. Chi *et al.* has demonstrated twin-free growth of GaAs NSs by selective area growth.¹⁹

A key question associated with nanostructures such as NS grown on a lattice-mismatched substrate is to what extent the heterostructures can be grown coherently without generating misfit dislocations (MFDs) at the interfaces.¹³ Such an interfacial lattice defect can relieve strain to reduce the strain energy but with the positive energy penalty associated with the dislocation core. For larger nanostructures, the strain-energy contribution begins to dominate, and accordingly MFDs are generated above a critical size.¹³ Previous theoretical works based on continuum elasticity have addressed this issue and estimated the critical height and diameter of NW for MFD generation.^{20–24} In this paper, we address the issue for NS using atomistic simulations. Namely, combined molecular dynamics (MD) and quantum mechanical (QM) simulations are used to study the trade-off between strain-relief and dislocation-core energies for a GaAs NS on a Si substrate.

Another fundamental question regarding MFD is what are their effects on the interfacial electronic structure and consequently on the device performance. For example, dangling bonds at MFD cores introduce recombination mechanisms for charge carriers. The resulting charge accumulation at the interface also causes the pinning of the Fermi energy and the bending of the electronic energy band to affect the carrier transport.²⁵ Here, we perform a combined MD/QM study of charge redistribution and band bending due to a MFD at a GaAs/Si interface.

The rest of the paper is organized as follows: Section II describes simulation methods, and simulation results on the

critical size for MFD generation are presented in Sec. III. Section IV discusses the effects of MFDs on electronic properties, and Sec. V contains summary.

II. SIMULATION METHODS

MD simulations are performed on parallel computers using our parallel MD program.²⁶ The interatomic potential for GaAs (Refs. 27 and 28) consists of two- and three-body terms, where the two-body term accounts for steric repulsion as well as Coulombic, charge-dipole, and dipole-dipole interactions, and the three-body term describes bond stretching and bond bending.²⁹ The interatomic potential has been validated against various experimental and QM calculation results for the lattice constants and cohesive energies of various crystalline phases, elastic constants, surface energies, vibrational density of states (DOS), thermal expansion coefficient, specific heat, and melting temperature.^{27,28} In particular, the interatomic potential reproduces the contraction of Ga-As bonds near the (110) surface of the zinc-blende (ZB) crystal, in agreement with QM results.¹⁷ This is important since GaAs NSs have {110} sidewall surfaces.¹⁹ For Si, we have chosen the Stillinger-Weber interatomic potential, which provides a reasonable description of crystalline Si.³⁰

To describe GaAs/Si interfaces, we employ a scheme that combines the interatomic potentials for GaAs and Si. A similar environment-dependent linear interpolation scheme has been used successfully to study lattice mismatched GaAs/InAs (Refs. 31 and 32) and Si₃N₄/Si (Refs. 33 and 34) interfaces. For Ga-Si and As-Si pair interactions, we adopt a simple two-parameter interpolation formula

$$v_{\text{Ga-Si}}^{(2)}(r) = w_{\text{Ga}} v_{\text{Ga-As}}^{(2)}(r) + (1 - w_{\text{Ga}}) v_{\text{Si-Si}}^{(2)}(r), \quad (1)$$

$$v_{\text{As-Si}}^{(2)}(r) = w_{\text{As}} v_{\text{Ga-As}}^{(2)}(r) + (1 - w_{\text{As}}) v_{\text{Si-Si}}^{(2)}(r), \quad (2)$$

where r is the interatomic distance, $v_{\text{Ga-As}}^{(2)}(r)$ is the Ga-As pair interaction term in the GaAs interatomic potential,^{27,28} and $v_{\text{Si-Si}}^{(2)}(r)$ is the Si-Si pair interaction term in the Stillinger-Weber potential.³⁰

The two parameters, w_{Ga} and w_{As} in Eqs. (1) and (2), are determined to best reproduce QM interatomic forces. To do so, we first prepare a GaAs/Si interface by stacking slabs of GaAs ZB crystal and Si diamond crystal with (111) surfaces (Fig. 1), in which the GaAs/Si interface consists of an As-Si bilayer (enclosed by the dashed square in Fig. 1) as in experimental systems.¹⁹ The system size is $13.3 \text{ \AA} \times 7.68 \text{ \AA} \times 81.44 \text{ \AA}$ in the x , y , and z directions (or $[1\bar{1}0]$, $[11\bar{2}]$, and $[111]$ crystallographic orientations). To represent coherent GaAs layers deposited on a Si substrate, the lateral simulation box size is determined by the Si lattice constant. Consequently, the GaAs slab is compressed by 3.9% in the x and y directions. Periodic boundary conditions (PBCs) are applied to all Cartesian directions. The simulated system contains 72 Ga, 80 As, and 120 Si atoms (in total of 288 atoms).

To provide a reference system to fit the adjustable parameters in the MD interatomic potential, we perform QM calculation³⁵ based on the density functional theory (DFT),³⁶ in which interatomic forces are computed quantum

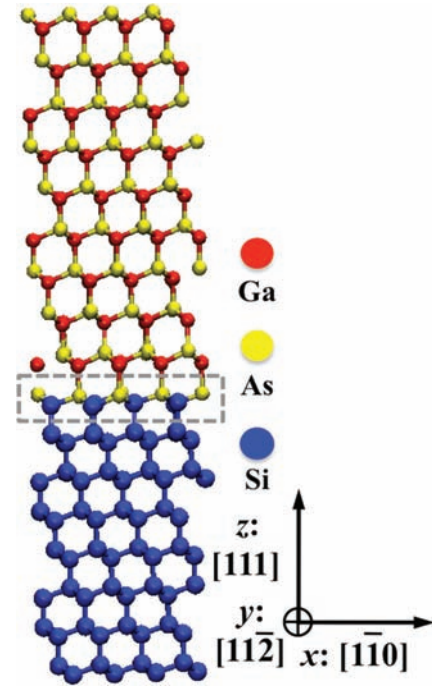


FIG. 1. The simulated GaAs/Si interface, where red, yellow, and blue spheres represent Ga, As, and Si atoms, respectively.

mechanically based on the Feynman-Hellmann theorem. In the QM calculation, the electronic states are calculated using the projector-augmented-wave method,^{37,38} which is an all-electron electronic-structure-calculation method within the frozen-core approximation. The generalized gradient approximation³⁹ is used for the exchange-correlation energy with non-linear core corrections.⁴⁰ The momentum-space formalism is utilized,⁴¹ where the plane-wave cutoff energies are 30 and 250 Ry for the electronic pseudo-wave functions and the pseudo-charge density, respectively. The energy functional is minimized iteratively using a preconditioned conjugate-gradient method.^{42,43} The Γ point is used for Brillouin zone sampling. Projector functions are generated for the 4s, 4p, and 4d states of Ga and As, and for the 3s, 3p, and 3d states for Si. The minimum-energy atomic configuration is obtained by relaxing the atomic positions using the quasi Newton method.

In the relaxed configuration, quantum-mechanically computed forces acting on all atoms are zero. For this configuration, we use the MD interatomic potential in Eqs. (1) and (2) to compute MD interatomic forces \mathbf{F}_i for all atoms i . The parameters, w_{Ga} and w_{As} , are determined to minimize the squared sum of the MD forces, i.e., deviation of the MD forces from the QM forces

$$(w_{\text{Ga}}^*, w_{\text{As}}^*) = \operatorname{argmin}_{w_{\text{Ga}}, w_{\text{As}}} \left(\sum_{i=1}^N |\mathbf{F}_i(w_{\text{Ga}}, w_{\text{As}})|^2 \right), \quad (3)$$

where N is the number of atoms.

Figure 2 shows the squared sum of the MD forces as a function of the force interpolation parameters, w_{Ga} and w_{As} . From this result, we choose the optimal parameters to minimize the deviation from the QM forces as $w_{\text{Ga}} = 0.0$ and $w_{\text{As}} = 0.6$.

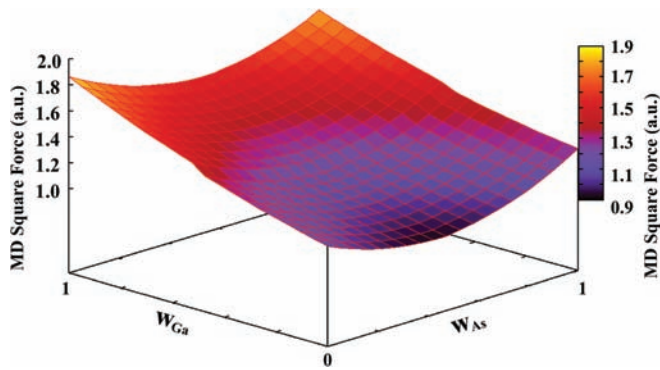


FIG. 2. Squared sum of the MD forces as a function of w_{Ga} and w_{As} for the GaAs/Si interface in Fig. 1.

Regarding the interpolation of the three-body interactions at GaAs/Si interfaces, we adopt a simple scheme. Namely, for three-body interactions involving Si as one of the triplet of atoms, we use the Stillinger-Weber three-body term for Si.³⁰ This may be justified since all the three-body terms have the same functional form and contain the identical bond-angle constant.

III. CRITICAL SIZE FOR MISFIT-DISLOCATION GENERATION

Using the QM-informed MD interatomic potential described in Sec. II, we perform MD simulation of a GaAs NS with thickness W and height H on Si (111) substrate (see Fig. 3). Here, W ranges from 4 to 58 nm, and H ranges from 3 to 40 nm. The x , y , and z axes are along the $[1\bar{1}0]$, $[11\bar{2}]$, and $[111]$ crystallographic orientations, respectively. The normal direction of the $(1\bar{1}0)$ NS sidewall surface is in the x direction. The size of the Si substrate is $3W \times 13.3 \text{ nm} \times W$ in the x , y and z directions, and that of the GaAs NS is $W \times 13.3 \text{ nm} \times H$ nm in the x , y , and z directions. PBCs are applied in the x and y directions.

We perform MD simulations for two sets of systems (without and with a MFD). In the former (coherent systems), the GaAs lattice is placed commensurate to the underlying Si lattice. In the latter (incoherent systems), a MFD core is inserted in the middle of the NS by creating a misalignment of the GaAs and Si lattices. The thread of the MFD is oriented in the $[11\bar{2}]$ direction, and the Burgers vector is in the $[1\bar{1}0]$ direction. Starting from each initial configuration, the atomic configuration is relaxed using the conjugate-gradient method to obtain the local minimum-energy configuration.

Figures 3(a) and 3(b) show the color-coded hydrostatic stress distribution without and with MFD, respectively, where $W = 10 \text{ nm}$ and $H = 20 \text{ nm}$. With the MFD, the spatial extent of highly stressed region is reduced. The compressive region above 1 GPa in the GaAs NS extends up to a height of 7.2 nm without MFD, and this height is reduced to 4.0 nm with MFD. Similarly, the tensile region below -1 GPa in the Si substrate reaches a depth of 8.6 and 6.0 nm, respectively, without and with MFD. This result confirms considerable stress relief by MFD, which was predicted by continuum elasticity calculations.^{20–24}

To quantify the strain-energy release along with the dislocation-core energy introduced by the MFD, we calculate the energy difference ΔE between the systems with and without MFD and plot it as a function of the NS thickness W , where H is fixed at 20 nm (see Fig. 4). For small W , the positive energy associated with the dislocation core dominates and thus the energy change due to the introduction of MFD is positive. For larger W ($> 10 \text{ nm}$), the strain-energy release exceeds the dislocation-core energy and the energy change due to the introduction of a MFD becomes negative. Namely, for thicker GaAs NSs on Si substrate, MFD generation is an energetically favorable process. Below the critical thickness of $W_c \sim 10 \text{ nm}$, on the other hand, GaAs NS can be grown coherently without interfacial defects. This is consistent with experimental observations by Tomioka *et al.* for GaAs NWs grown on Si.¹³ For small diameters, coherent

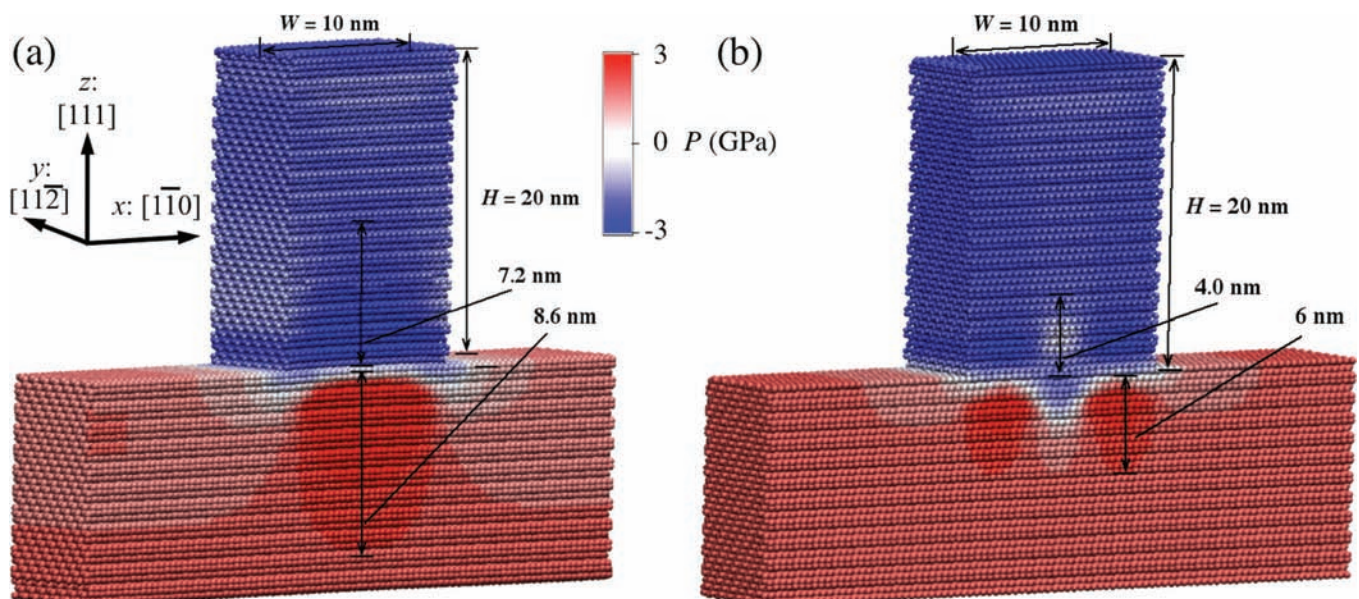


FIG. 3. Stress distribution in a GaAs NS on Si substrate without (a) and with (b) MFD. The hydrostatic stress is color-coded.

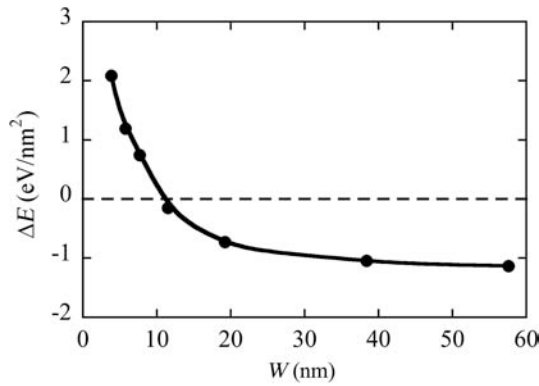


FIG. 4. Energy difference between the systems with and without MFD as a function of the NS thickness W .

GaAs NWs without MFD were observed, whereas for larger diameters a periodic array of MFDs with a period of ~ 8 nm were observed. The calculated critical NS thickness of 10 nm is consistent with these observations. For a slightly different geometry, i.e., an axial heterostructure NW with 4% lattice mismatch (as for GaAs/Si), continuum elasticity calculation predicts a critical diameter of $D_c \sim 20$ nm, below which coherent growth is possible without MFD.²¹ Above D_c , the continuum elasticity calculation also predicts a critical height H_c of NW, below which the coherent growth is still possible. The calculated H_c is a few nm, where the applicability of continuum elasticity is questionable. In the case of NS, one may expect the existence of a similar critical height H_c for $W > W_c$, such that $\Delta E(W, H) > 0$ only for $H < H_c$ (and $\Delta E(W, H) \leq 0$ for $H \geq H_c$). Such critical height H_c , if exists, should rapidly diverge to infinity as W approaches W_c from above, and remains ∞ for all $W < W_c$, so that coherent growth is energetically favorable for all heights at subcritical widths. In our MD simulations with H varying from 3 to 40 nm for each W , however, we have not observed the change of sign for ΔE , i.e., the existence of H_c .

IV. EFFECTS OF MISFIT DISLOCATIONS ON ELECTRONIC PROPERTIES

We now study the effects of MFD on electronic properties at the GaAs/Si interface. As a reference system, we first study quantum mechanically the coherent GaAs/Si interface without MFD in Fig. 1. Figure 5 shows the electronic charge density at the interface. In the Si side, the charge density reflects the tetrahedral sp^3 bonding in its diamond crystal structure. On the other hand, the charge density in the GaAs side exhibits a drastically different symmetry. This is understandable, since the conduction band (CB) and valence band (VB) in GaAs have s- and p-type symmetry, respectively. To understand the nature of wave functions in GaAs, we have projected the electronic wave function at the conduction-band edge, $\psi_c(\mathbf{r})$, and those for the three hole bands $\psi_{h,\alpha}(\mathbf{r})$ ($\alpha = \text{heavy, light, and split-off}$) at the valence-band edge onto the wave functions of the pseudoatomic orbitals centered at Ga and As atoms.⁴⁴ For the conduction-band edge wave function, $\psi_c(\mathbf{r})$, 67.6% and 32.4% of the total population come from Ga 4s and As 4s states, respectively. The

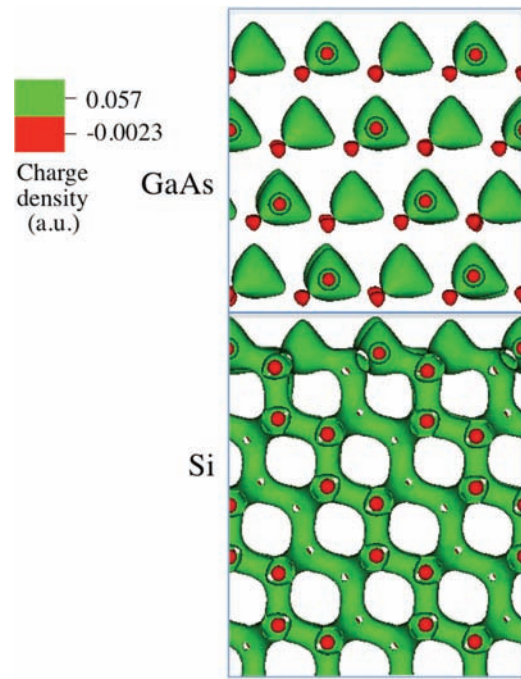


FIG. 5. Electron charge density at the GaAs/Si interface viewed from the [112] direction. Green and red surfaces represent contours with 0.057 and -0.0023 a.u., respectively.

partial populations of the three valence-band edge wave functions, $\psi_{h,\alpha}(\mathbf{r})$, are nearly identical: 80.3% and 11.6%, respectively, from As 4p and Ga 4p states. Namely, the conduction-band wave function is s-like and is centered at Ga atoms, whereas the valence-band wave functions are p-like around As atoms.

To quantify the change in the bonding properties of atoms at the interface, we use a bond-overlap population analysis^{45,46} by expanding the electronic wave functions with an atomic-orbital basis set.^{47,48} Based on the formulation generalized to the PAW method,⁴⁴ we obtain the gross population Z_i for the i th atom, from which we estimate the charge of atoms. As the atomic-basis orbitals, we use numerical eigenfunctions of atoms, which are obtained for a chosen atomic energy so that the first node occurs at the desired cut-off radius.⁴⁹ To increase the efficiency of the expansion, the numerical basis orbitals are augmented with the split-valence method.⁵⁰ The resulting charge spillage, which estimates the error in the expansion, is only 0.3%, indicating the high quality of the basis orbitals.

Figure 6(a) shows the atomic configuration at the GaAs/Si interface, where atomic charges are color-coded. In the As-Si bilayer at the interface, Si atoms are negatively charged while As atoms are nearly neutral. This indicates significant charge transfer from As to Si atoms in the interfacial As-Si bilayer. To highlight this effect, Fig. 6(b) shows the atomic charge versus the z coordinate for Ga (red triangle), As (yellow square) and Si (blue circle) atoms. The As and Si charges in the As-Si bilayer at $z \sim 25$ Å indeed show positive and negative shifts from their respective bulk values, confirming the charge transfer from As to Si. Furthermore, we observe positive shifts of the Ga and As charges in the

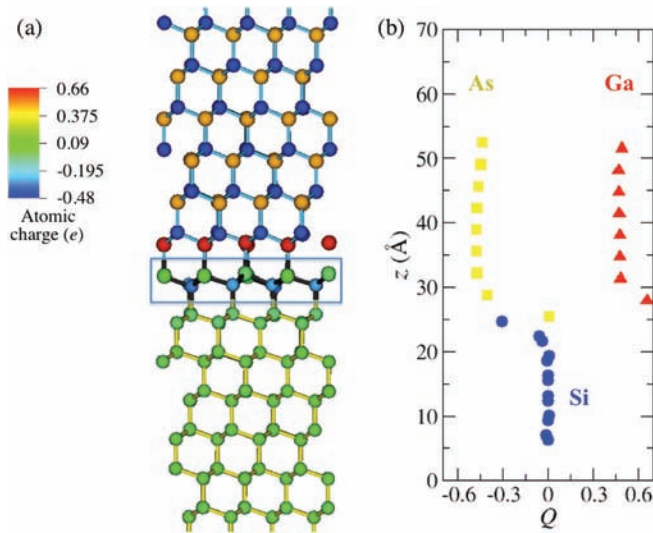


FIG. 6. Atomic charges at the GaAs/Si interface. (a) Color-coded atomic charges viewed from the [112] direction, where the interfacial As-Si bilayer is enclosed by a rectangle. (b) The atomic charge versus the z coordinate of Ga (red triangle), As (yellow square), and Si (blue circle) atoms.

Ga-As bilayer at $z \sim 29$ Å, indicating cross-bilayer charge transfer from the GaAs side to the Si side at the interface. This creates an interfacial dipole pointing from Si to GaAs.

Having studied electronic properties at a GaAs/Si interface, we now study how a MFD modifies the interfacial electronic properties. To prepare a MFD configuration for QM calculations, we cut out a small subset of atoms near the dislocation core from MD simulation of a GaAs NS on Si substrate (see Fig. 3(b)). This procedure generates dangling bonds at the xz -periphery of the cutout cluster, which are terminated by adding hydrogen atoms (see Fig. 7(a)). Note that PBC is still applied to the y direction, i.e., parallel to the MFD thread direction. The atomic configuration of the cluster containing 412 atoms (60 Ga, 84 As, 100 Si, and 168 H) is then relaxed using QM calculation to obtain the minimum-

energy configuration. The relaxation using the quasi-Newton method is performed in two steps: First, the positions of all Ga, As and Si atoms are fixed, and the H-atom positions are relaxed; subsequently, the positions of the H atoms as well as those of the Ga, As and Si atoms in the outermost layer of the cluster are fixed, and the positions of all the other atoms in the interior of the cluster are relaxed using QM forces. This provides quantum-mechanically accurate description of the MFD core embedded in a realistic long-range strain field.

Figure 7(a) shows the relaxed MFD configuration. At the dislocation core, there are a number of Ga and As atoms with dangling bonds. These dangling orbitals are expected to provide energy levels within the bulk band gap, thereby creating local charge density.²⁵ To show the charge redistribution at the MFD core, we calculate the change of atomic charges due to the introduction of MFD. From the atomic charge of each atom in Fig. 7(a), we subtract the charge of an atom of the same species (Ga, As, or Si) in the corresponding atomic layer in Fig. 6. Figure 7(b) shows the atomic-charge change ΔQ versus the z coordinate of Ga (red triangle), As (yellow square), and Si (blue circle) atoms averaged over each atomic monolayer. We observe a positive shift ΔQ of atomic charge due to MFD for Si in the As-Si bilayer below the interface (denoted by the dashed lines in Figs. 7(a) and 7(b)). This, along with the negative ΔQ for Ga in the Ga-As bilayer above the interface, is likely due to the reduction of cross-bilayer charge transfer from GaAs to Si because of the broken cross-bilayer bonds due to MFD (see Fig. 7(a)). The reduced cross-bilayer charge transfer from Ga also results in the positive ΔQ for As in the As-Si bilayer below the interface. Such interfacial charge redistribution due to MFD is expected to influence carrier transport significantly.²⁵

Next, we study the bending of energy bands at the GaAs/Si interface. This can be done by calculating the partial electronic DOS $D_n(E)$ projected onto the wave functions of the atoms in the n -th (111) atomic bilayer along the z axis;⁵¹ see Figs. 8(a) and 8(c) for the numbering of bilayers, respectively, in the cases without and with MFD. Figures 8(b) and 8(d) show $D_n(E)$ (red curves) without and with MFD, respectively, where the upper and lower blue lines denote the CB and VB edges, respectively. Here, we have applied self-interaction correction to the energies of the Kohn-Sham orbitals.⁵² For the coherent interface, Fig. 8(b) shows the change of the band gap from 1 to 1.5 eV when moving from the Si to the GaAs side. However, the CB and VB edge positions do not change monotonically from the Si side to the GaAs side. Namely, both exhibit an extremum at the As-Si bilayer (i.e., the bilayer number 4). This non-monotonic energy band profile is likely due to the distinct chemical environment and the charge transfer in the As-Si bilayer (labeled 4 in Figs. 8(a) and 8(b)). The interfacial strain due to the lattice mismatch may also contribute to this behavior. Such a unique feature could significantly affect the carrier transport across the interface. With the introduction of MFD, Fig. 8(d) shows a more monotonic change of the CB and VB edges across the interface. This can be partially attributed to the reduced cross-bilayer charge transfer as well as strain relaxation at the MFD core.

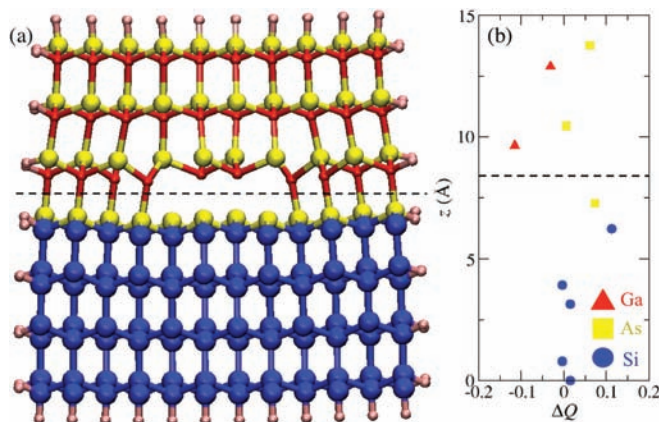


FIG. 7. (a) Relaxed MFD configuration with quantum-mechanical forces, where red, yellow, blue, and magenta spheres represent Ga, As, Si, and terminating H atoms, respectively. (b) The atomic-charge change due to MFD versus the z coordinate of Ga (red triangle), As (yellow square), and Si (blue circle) atoms averaged over each atomic monolayer. The dashed lines in (a) and (b) mark the interface.

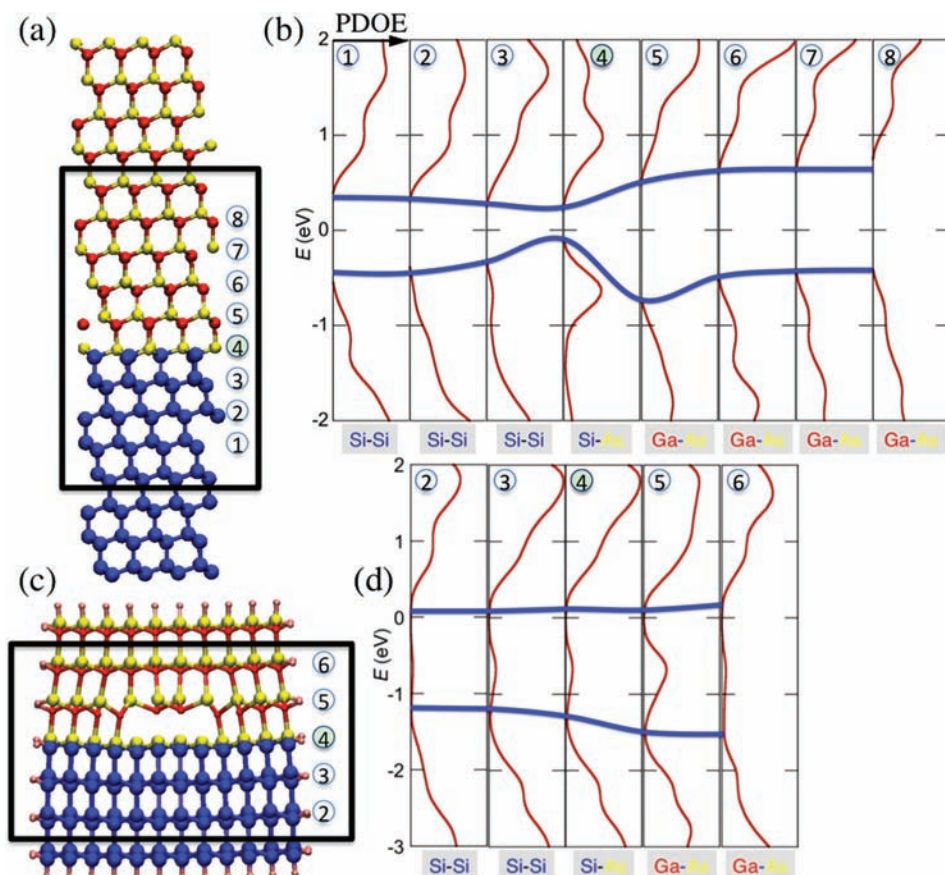


FIG. 8. (a) Numbering of atomic bilayers around the GaAs/Si interface without MFD, where red, yellow and blue spheres represent Ga, As and Si atoms. (b) Partial electronic densities-of-states (red curves) projected onto (111) atomic bilayers without MFD, where the upper and lower blue lines denote the conduction and valence band edges, respectively. (c) Numbering of atomic bilayers around the GaAs/Si interface with MFD. (d) Partial electronic densities-of-states projected onto atomic bilayers with MFD.

V. SUMMARY

In summary, we have used combined MD and QM simulations to study the generation of MFD in a GaAs NS on Si (111) substrate. We estimated the critical NS size, below which MFD-free growth is possible. We found considerable charge transfer from GaAs to Si at a GaAs/Si (111) interface. The charge transfer is reduced at the MFD core, which has a significant effect on the electronic band profile. These effects should have profound impacts on the efficiency of lattice-mismatched NS devices.

ACKNOWLEDGMENTS

This work was supported by the U.S. Department of Energy, Office of Science, Office of Basic Energy Sciences under Award No. DE-SC0001013 as part of the Center for Energy Nanoscience, an Energy Frontier Research Center. Simulations were performed at the Center for High Performance Computing and Communications of the University of Southern California.

¹M. Law, L. E. Greene, J. C. Johnson, R. Saykally, and P. D. Yang, *Nature Mater.* **4**(6), 455–459 (2005).

²J. Wallentin, N. Anttu, D. Asoli, M. Huffman, I. Aberg, M. H. Magnusson, G. Siefert, P. Fuss-Kailuweit, F. Dimroth, B. Witzigmann, H. Q. Xu, L. Samuelson, K. Deppert, and M. T. Borgstrom, *Science* **339**(6123), 1057–1060 (2013).

³T. Zhu and J. Li, *Prog. Mater. Sci.* **55**(7), 710–757 (2010).

⁴J. R. Greer and J. T. M. De Hosson, *Prog. Mater. Sci.* **56**(6), 654–724 (2011).

⁵Y. B. Wang, H. J. Joyce, Q. A. Gao, X. Z. Liao, H. H. Tan, J. Zou, S. P. Ringer, Z. W. Shan, and C. Jagadish, *Nano Lett.* **11**(4), 1546–1549 (2011).

⁶W. Shockley and H. J. Queisser, *J. Appl. Phys.* **32**(3), 510–519 (1961).

⁷K. Tomioka, J. Motohisa, S. Hara, K. Hiruma, and T. Fukui, *Nano Lett.* **10**(5), 1639–1644 (2010).

⁸J. H. Kang, Q. Gao, P. Parkinson, H. J. Joyce, H. H. Tan, Y. Kim, Y. Guo, H. Xu, J. Zou, and C. Jagadish, *Nanotechnology* **23**(41), 415702 (2012).

⁹W. Wei, X. Y. Bao, C. Soci, Y. Ding, Z. L. Wang, and D. Wang, *Nano Lett.* **9**(8), 2926–2934 (2009).

¹⁰K. Tomioka, M. Yoshimura, and T. Fukui, *Nature* **488**(7410), 189–192 (2012).

¹¹M. Heurlin, P. Wickert, S. Falt, M. T. Borgstrom, K. Deppert, L. Samuelson, and M. H. Magnusson, *Nano Lett.* **11**(5), 2028–2031 (2011).

¹²T. Martensson, C. P. T. Svensson, B. A. Wacaser, M. W. Larsson, W. Seifert, K. Deppert, A. Gustafsson, L. R. Wallenberg, and L. Samuelson, *Nano Lett.* **4**(10), 1987–1990 (2004).

¹³K. Tomioka, T. Tanaka, S. Hara, K. Hiruma, and T. Fukui, *IEEE J. Sel. Top. Quantum Electron* **17**(4), 1112–1129 (2011).

¹⁴K. Tomioka, K. Ikejiri, T. Tanaka, J. Motohisa, S. Hara, K. Hiruma, and T. Fukui, *J. Mater. Res.* **26**(17), 2127–2141 (2011).

¹⁵D. Rudolph, S. Hertenberger, S. Bolte, W. Paosangthong, D. Spirkoska, M. Doblinger, M. Bichler, J. J. Finley, G. Abstreiter, and G. Koblmüller, *Nano Lett.* **11**(9), 3848–3854 (2011).

¹⁶F. Glas, J. C. Harmand, and G. Patriarche, *Phys. Rev. Lett.* **99**(14), 146101 (2007).

¹⁷Z. Yuan, K. Nomura, and A. Nakano, *Appl. Phys. Lett.* **100**(16), 163103 (2012).

¹⁸K. Ikejiri, T. Sato, H. Yoshida, K. Hiruma, J. Motohisa, S. Hara, and T. Fukui, *Nanotechnology* **19**(26), 265504 (2008).

¹⁹C.-Y. Chi, C.-C. Chang, S. Hu, T.-W. Yeh, S. B. Cronin, and P. D. Dapkus, *Nano Lett.* **13**(6), 2506–2515 (2013).

²⁰E. Ertekin, P. A. Greaney, D. C. Chrzan, and T. D. Sands, *J. Appl. Phys.* **97**(11), 114325 (2005).

²¹F. Glas, *Phys. Rev. B* **74**(12), 121302 (2006).

²²S. Raychaudhuri and E. T. Yu, *J. Appl. Phys.* **99**(11), 114308 (2006).

²³S. Surlan, A. Nakano, and P. D. Dapkus, *J. Appl. Phys.* **111**(5), 054907 (2012).

- ²⁴S. Sburian, P. D. Dapkus, and A. Nakano, *Appl. Phys. Lett.* **100**(16), 163108 (2012).
- ²⁵V. Gopal, E. P. Kvam, T. P. Chin, and J. M. Woodall, *Appl. Phys. Lett.* **72**(18), 2319–2321 (1998).
- ²⁶A. Nakano, R. K. Kalia, K. Nomura, A. Sharma, P. Vashishta, F. Shimojo, A. C. T. van Duin, W. A. Goddard, R. Biswas, D. Srivastava, and L. H. Yang, *Int. J. High Perform Comput. Appl.* **22**(1), 113–128 (2008).
- ²⁷S. Kodiyalam, R. K. Kalia, H. Kikuchi, A. Nakano, F. Shimojo, and P. Vashishta, *Phys. Rev. Lett.* **86**(1), 55–58 (2001).
- ²⁸S. Kodiyalam, R. K. Kalia, A. Nakano, and P. Vashishta, *Phys. Rev. Lett.* **93**(20), 203401 (2004).
- ²⁹P. Vashishta, R. K. Kalia, J. P. Rino, and I. Ebbsjo, *Phys. Rev. B* **41**(17), 12197–12209 (1990).
- ³⁰F. H. Stillinger and T. A. Weber, *Phys. Rev. B* **31**(8), 5262–5271 (1985).
- ³¹X. Su, R. K. Kalia, A. Nakano, P. Vashishta, and A. Madhukar, *Appl. Phys. Lett.* **78**(23), 3717–3719 (2001).
- ³²X. Su, R. K. Kalia, A. Nakano, P. Vashishta, and A. Madhukar, *Appl. Phys. Lett.* **79**(27), 4577–4579 (2001).
- ³³A. Omeltchenko, M. E. Bachlechner, A. Nakano, R. K. Kalia, P. Vashishta, I. Ebbsjo, A. Madhukar, and P. Messina, *Phys. Rev. Lett.* **84**(2), 318–321 (2000).
- ³⁴M. E. Bachlechner, A. Omeltchenko, A. Nakano, R. K. Kalia, P. Vashishta, I. Ebbsjo, and A. Madhukar, *Phys. Rev. Lett.* **84**(2), 322–325 (2000).
- ³⁵F. Shimojo, S. Ohmura, R. K. Kalia, A. Nakano, and P. Vashishta, *Phys. Rev. Lett.* **104**(12), 126102 (2010).
- ³⁶P. Hohenberg and W. Kohn, *Phys. Rev.* **136**(3B), B864–B871 (1964).
- ³⁷P. E. Blochl, *Phys. Rev. B* **50**(24), 17953–17979 (1994).
- ³⁸G. Kresse and D. Joubert, *Phys. Rev. B* **59**(3), 1758–1775 (1999).
- ³⁹J. P. Perdew, K. Burke, and M. Ernzerhof, *Phys. Rev. Lett.* **77**(18), 3865–3868 (1996).
- ⁴⁰S. G. Louie, S. Froyen, and M. L. Cohen, *Phys. Rev. B* **26**(4), 1738–1742 (1982).
- ⁴¹J. Ihm, A. Zunger, and M. L. Cohen, *J. Phys. C* **12**(21), 4409–4422 (1979).
- ⁴²G. Kresse and J. Hafner, *Phys. Rev. B* **49**(20), 14251–14269 (1994).
- ⁴³F. Shimojo, R. K. Kalia, A. Nakano, and P. Vashishta, *Comput. Phys. Commun.* **140**(3), 303–314 (2001).
- ⁴⁴F. Shimojo, A. Nakano, R. K. Kalia, and P. Vashishta, *Phys. Rev. E* **77**(6), 066103 (2008).
- ⁴⁵R. S. Mulliken, *J. Chem. Phys.* **23**(10), 1833–1840 (1955).
- ⁴⁶R. S. Mulliken, *J. Chem. Phys.* **23**(10), 1841–1846 (1955).
- ⁴⁷D. Sánchez-Portal, E. Artacho, and J. M. Soler, *J. Phys.: Condens. Matter* **8**(21), 3859–3880 (1996).
- ⁴⁸M. D. Segall, R. Shah, C. J. Pickard, and M. C. Payne, *Phys. Rev. B* **54**(23), 16317–16320 (1996).
- ⁴⁹O. F. Sankey and D. J. Niklewski, *Phys. Rev. B* **40**(6), 3979–3995 (1989).
- ⁵⁰J. M. Soler, E. Artacho, J. D. Gale, A. García, J. Junquera, P. Ordejón, and D. Sánchez-Portal, *J. Phys.: Condens. Matter* **14**(11), 2745–2779 (2002).
- ⁵¹W. Mou, S. Ohmura, F. Shimojo, and A. Nakano, *Appl. Phys. Lett.* **100**(20), 203306 (2012).
- ⁵²F. Shimojo, S. Ohmura, W. Mou, R. K. Kalia, A. Nakano, and P. Vashishta, *Comput. Phys. Commun.* **184**(1), 1–8 (2013).